Gamow-Teller strength distributions at finite temperatures and electron capture in stellar environments

Alan A. Dzhioev,[1,*] A. I. Vdovin,[1] V. Yu. Ponomarev,[2] J. Wambach,[2,3] K. Langanke,[2,3,4] and G. Martínez-Pinedo[3]

[1]*Bogoliubov Laboratory of Theoretical Physics, Joint Institute for Nuclear Research, RU-141980 Dubna, Russia*

[2]*Institut für Kernphysik, Technische Universität Darmstadt, D-64289 Darmstadt, Germany*

[3]*GSI Helmholtzzentrum für Schwerionenforschung, Planckstr. 1, D-64291 Darmstadt, Germany*

[4]*Frankfurt Institute for Advanced Studies, Ruth-Moufang Strasse 1, D-60438 Frankfurt, Germany*

We propose a new method to calculate stellar weak-interaction rates. It is based on the thermofield dynamics formalism and allows calculation of the weak-interaction response of nuclei at finite temperatures. The thermal evolution of the GT_+ distributions is presented for the sample nuclei ^{54,56}Fe and ^{76,78,80}Ge. For Ge we also calculate the strength distribution of first-forbidden transitions. We show that thermal effects shift the GT_+ centroid to lower excitation energies and make possible negative- and low-energy transitions. In our model we demonstrate that the unblocking effect for GT_+ transitions in neutron-rich nuclei is sensitive to increasing temperature. The results are used to calculate electron capture rates and are compared to those obtained from the shell model.

PACS number(s): 26.50.+x, 23.40.−s, 21.60.Jz, 24.10.Pa

I. INTRODUCTION

The properties of nuclei at finite temperatures have attracted attention for a long time. Because of the considerable amount of experimental data the main subject of study has been the thermal properties of giant dipole resonance (see, e.g., Refs. [1] and [2] and references therein). In the astrophysical context the thermal properties of Gamow-Teller (GT) transitions are of special interest, as they play a crucial role in weak-interaction-mediated reactions [electron capture (EC), β decay, neutrino scattering, etc.] [3]. For example, EC on iron-group nuclei initiates the gravitational collapse of the core of a massive star, triggering a supernova explosion. Moreover, EC rates largely determine the mass of the core and thus the fate of the shock wave formed by the supernova explosion. Because the strong phase-space dependence makes the relevant stellar weak-interaction rates at the early stage of the collapse—when the electron chemical potential μ_e is of the same order as the nuclear Q values—very sensitive to the GT distributions, these need to be calculated very accurately in this regime. With proceeding collapse and hence increasing density, μ_e grows more rapidly than the Q values of the nuclei present in the matter composition, and the capture rates become less sensitive to the details of the GT distribution and are mainly determined by the total GT strength and its centroid energy. However, forbidden transitions can no longer be neglected when μ_e reaches values of the order of 30 MeV at core densities $\rho > 10^{11}$ g/cm^3 [3,4] The situation is further complicated by the fact that weak-interaction processes in stellar environments take place at temperatures of the order of a few hundred kilo–electron volts to a few mega–electron volts and GT transitions occur not only from the nuclear ground state, but also from excited states.

From a microscopic point of view, there are two routes for handling GT strength distributions and weak-interaction rates at finite temperatures. One is a state-by-state evaluation of the rate by summing over Boltzmann-weighted, individually determined GT strengths for the various states. The second is based on an equilibrium statistical formulation of the nuclear many-body problem. In this approach, the thermal response of a nucleus to an external perturbing field is given by the canonical (or grand canonical) expectation value of the corresponding transition operator. When applied to charge-exchange processes this method yields the temperature-dependent GT and first-forbidden (FF) strength function, which can be then used to calculate weak-interaction rates.

For sd- and pf-shell nuclei the first approach was originally used by Fuller *et al.* [5], who calculated stellar weak-interaction rates using the independent-particle shell model, supplemented by experimental data whenever available. To allow for GT transitions from nuclear excited states these authors employed the Brink hypothesis. This assumes that the GT strength distribution for excited states is the same as for the ground state, only shifted by the excitation energy of the state. These rates were subsequently updated, taking into account the quenching of the axial coupling constant [6]. Modern high-performance computing capabilities combined with state-of-the-art diagonalization approaches make possible shell-model calculations of the GT strength distribution not only for the nuclear ground state, but also for the few lowest excited states. It was demonstrated [7,8] that even for the lowest excited states in the parent nucleus the Brink hypothesis is valid only for the bulk of the GT strength, and is not applicable for the individual transitions to states at a low excitation energy in the daughter nucleus. Taking this into account, weak-interaction rates based on the shell-model diagonalization approach [9,10] were derived from the individual GT distributions from the lowest excited states and from "back-resonant contributions," that is, from transitions determined from the inverse GT distributions connecting excited states in the daughter spectrum to the

*dzhioev@theor.jinr.ru

lowest states in the parent spectrum. However, the compilation of Refs. [9] and [10] applied Brink's hypothesis when taking into account GT transitions from highly excited states. Weak-interaction rates have also been computed using the spectral distribution theory [11] and the proton-neutron quasiparticle random-phase approximation (RPA) model [12]. The first method is also based on the Brink hypothesis. The latter does not use this hypothesis, but some uncertainties arise owing to the approximate treatment of the parent excited states as multiquasiparticle states as well as the insufficient knowledge of the quantum numbers of the states involved. Recently, stellar EC rates were calculated within the framework of the finite-temperature RPA using a set of Skyrme interactions [13]. This method has the advantage of consistency, however, it misses relevant correlations that, as we demonstrate here, are crucial for deriving stellar EC rates for neutron-rich nuclei.

The statistical way to calculate temperature-dependent GT and FF strength functions was first applied in Ref. [4] to study EC on neutron-rich nuclei. The most advanced realization of this procedure is presently performed in the framework of the shell-model Monte Carlo (SMMC) method [14]. It was found [15] that, with increasing temperature, the GT centroids shift to lower excitation energies and the widths of the distributions increase with the appearance of low-lying strength. Both effects arise from thermally excited states, that is, the Brink hypothesis is not supported by SMMC calculations. Despite its advantages, the SMMC method yields only the lowest moments of the GT strength distributions, which introduce some inaccuracies into the rate calculations. Moreover, the SMMC method has restrictions in its applicability to odd-odd and odd-*A* nuclei at low temperatures.

Thus, the problem of an accurate description of the GT strength distribution at finite temperatures and reliable estimates of stellar weak-interaction rates is not solved completely yet: The shell-model diagonalization approach allows for detailed spectroscopy but partially employs the Brink hypothesis. The SMMC method is free of this disadvantage but cannot provide a detailed strength distribution. Moreover, present computer capabilities allow application of the shell-model diagonalization method only to nuclei in the iron region ($A = 45$–65), whereas the SMMC approach can be applied, in principle, to all nuclei. However, such calculations are rather time-consuming and have therefore been limited to about 200 nuclei with mass numbers $A = 65$–120 [3,16], although weak processes in more massive and neutron-rich nuclei also play an important role in various astrophysical scenarios. Therefore, alternative methods for dealing with GT strength distributions and weak-interaction rates at finite temperatures are desirable.

In this paper we study the temperature dependence of the GT strength by applying the proton-neutron quasiparticle RPA [17] extended to finite temperature by the thermofield dynamics (TFD) formalism [18,19]. This technique does not rely on Brink's hypothesis. The energies of the GT transitions and corresponding transition strengths are calculated as functions of the nuclear temperature. We apply this method to calculate rates of weak-interaction processes on iron-group nuclei and neutron-rich nuclei beyond the *pf* shell. However, the method is not restricted to these nuclei

but can be applied to heavier nuclei as well. It also allows calculation of the strength distributions of forbidden transitions that contribute significantly to weak-interaction rates at high densities. Although, in the present paper, we restrict our study to the one-phonon, that is, RPA, approach, the method can be extended to take into account multiphonon admixtures, thus yielding more detailed strength distributions.

The paper is organized as follows. In Sec. II, some important features of the TFD formalism with application to the nuclear structure problem at finite temperatures are presented. The thermal quasiparticle RPA (TQRPA) equations, which describe the strength distributions of charge-exchange transitions in hot nuclei, are given in Sec. II as well. In Sec. III the necessary formulas to calculate EC rates in a stellar environment are introduced. Results for the GT strength distributions and EC rates in ^{54,56}Fe are presented in Sec. IV. There we also compare the results with those from the shell-model diagonalization approach. In Sec. V, we study the temperature dependence of GT and FF strength distributions in the neutron-rich isotope ^{76}Ge. The corresponding EC cross sections and rates are calculated and compared with those obtained within the hybrid SMMC + RPA model [20]. Conclusions are drawn in Sec. VI.

II. FORMALISM

For study of the thermal behavior of quantum many-body systems, the TFD method has two attractive features: (a) temperature effects arise explicitly as *T*-dependent vertices, providing a convenient starting point for various approximations; and (b) temperature and time are independent variables. The first feature allows for straightforward extensions of well-established zero-temperature approximations. It has been employed previously in Refs. [21–25], where selected nuclear structure problems at finite temperatures were considered.

The standard TFD formalism treats a many-particle system in thermal equilibrium with a heat bath and a particle reservoir in the grand canonical ensemble. The thermal average of a given operator *A* is calculated as the expectation value in a specially constructed, temperature-dependent state $|0(T)\rangle$, which is termed the thermal vacuum. This expectation value is equal to the usual grand canonical average of *A*.

To construct the state $|0(T)\rangle$, a formal doubling of the system degrees of freedom is introduced. In TFD, a tilde conjugate operator $\widetilde{A}$—acting in the independent Hilbert space—is associated with *A*, in accordance with properly formulated tilde conjugation rules [18,19,26]. For a system governed by the Hamiltonian *H* the whole Hilbert space is now spanned by the direct product of the eigenstates of *H* ($H|n\rangle = E_n|n\rangle$) and those of the tilde Hamiltonian $\widetilde{H}$, both having the same eigenvalues ($\widetilde{H}|\widetilde{n}\rangle = E_n|\widetilde{n}\rangle$). In the doubled Hilbert space, the thermal vacuum is defined as the zero-energy eigenstate of the so-called thermal Hamiltonian $\mathcal{H} = H - \widetilde{H}$ and it satisfies the thermal-state condition [18,19,26]

$$A|0(T)\rangle = \sigma e^{\mathcal{H}/2T} \widetilde{A}^{\dagger}|0(T)\rangle, \tag{1}$$

where $\sigma = 1$ for bosonic *A* and $\sigma = i$ for fermionic *A*.

The important point is that in the doubled Hilbert space the time-translation operator is not the initial Hamiltonian *H*, but

the thermal Hamiltonian $\mathcal{H}$. This means that the excitations of the thermal system are obtained by the diagonalization of $\mathcal{H}$. As follows from the definition of $\mathcal{H}$, each of its eigenstates with positive energy has a counterpart—the tilde-conjugate eigenstate—with negative energy but the same absolute value. This is a way to treat excitation- and de-excitation processes at finite temperatures within TFD.

Obviously, in most practical cases one cannot diagonalize $\mathcal{H}$ exactly. Usually, one resorts to certain approximations such as the Hartree-Fock Bogoliubov mean field theory and the RPA (see, e.g., Ref. [22]). In what follows the formal part of the TFD studies for charge-exchange excitations in hot nuclei is based in part on the results of Refs. [27] and [28].

In the present study we use a phenomenological nuclear Hamiltonian consisting of a static mean field, Bardeen-Cooper-Schrieffer (BCS) pairing interactions, and separable multipole and spin-multipole particle-hole interactions, including isoscalar and isovector parts. This is usually referred to as the quasiparticle-phonon model (QPM) [29]. It was used to study the charge-exchange excitations in nuclei at zero temperature in Refs. [30] and [31]. In principle, the QPM formalism enables one to go beyond the QRPA and take into account the coupling of quasiparticles and phonons. At finite temperatures this coupling was considered in Refs. [24] and [27]. However, in the present study we restrict ourselves to the TQRPA.

The main line of the present discussion is very similar to the QPM at $T = 0$ [29]. We begin with the thermal Hamiltonian, which reads as

$$\mathcal{H}_{\text{QPM}} = H_{\text{QPM}} - \widetilde{H}_{\text{QPM}} = \mathcal{H}_{\text{sp}} + \mathcal{H}_{\text{pair}} + \mathcal{H}_{\text{ph}}. \quad (2)$$

The first step in the approximate diagonalization of $\mathcal{H}_{\text{QPM}}$ is the treatment of the pairing correlations. This is done by two successive unitary transformations. The first is the usual Bogoliubov u, v transformation from the original particle operators $a^\dagger_{jm}$, a_{jm} to the quasiarticle ones $\alpha^\dagger_{jm}$, α_{jm}. The same transformation is applied to tilde operators $\widetilde{a}^\dagger_{jm}$, $\widetilde{a}_{jm}$, thus producing the tilde quasiparticle operators $\widetilde{\alpha}^\dagger_{jm}$, $\widetilde{\alpha}_{jm}$.

The second transformation is the so-called thermal Bogoliubov transformation [18,19]. It mixes the quasiparticle and tilde quasiparticle operators, thus producing thermal quasiparticle operators and their tilde partners: $\beta^\dagger_{jm}$, β_{jm}, $\widetilde{\beta}^\dagger_{jm}$, and $\widetilde{\beta}_{jm}$. We use Ojima's [26] complex form of the thermal Bogoliubov transformation:

$$\begin{aligned} \beta^\dagger_{jm} &= x_j \alpha^\dagger_{jm} - i y_j \widetilde{\alpha}_{jm}, \\ \widetilde{\beta}^\dagger_{jm} &= x_j \widetilde{\alpha}^\dagger_{jm} + i y_j \alpha_{jm} \ (x_j^2 + y_j^2 = 1). \end{aligned} \quad (3)$$

The reasons for this are given in Ref. [27].

The coefficients u_j, v_j, x_j, and y_j are found by diagonalizing $\mathcal{H}_{\text{sp}} + \mathcal{H}_{\text{pair}}$ and demanding that the vacuum of thermal quasiparticles obeys the thermal-state condition (1). This is equivalent to the minimization of the thermodynamic potential for Bogoliubov quasiparticles. As a result one obtains the

following equations for u_j, v_j and x_j, y_j:

$$v_j = \frac{1}{\sqrt{2}} \left(1 - \frac{E_j - \lambda_\tau}{\varepsilon_j}\right)^{1/2}, \quad u_j = \left(1 - v_j^2\right)^{1/2}, \quad (4)$$

$$y_j = \left[1 + \exp\left(\frac{\varepsilon_j}{T}\right)\right]^{-1/2}, \quad x_j = \left(1 - y_j^2\right)^{1/2}, \quad (5)$$

where $\varepsilon_j = \sqrt{(E_j - \lambda_\tau)^2 + \Delta_\tau^2}$ and τ is the isospin quantum number $\tau = n, p$.

The pairing gap Δ_τ and the chemical potential λ_τ are the solutions to the finite-temperature BCS equations,

$$\begin{aligned} \Delta_\tau(T) &= \frac{G_\tau}{2} \sum_j^\tau (2j+1)\left(1 - 2y_j^2\right) u_j v_j, \\ N_\tau &= \sum_j^\tau (2j+1)\left(v_j^2 x_j^2 + u_j^2 y_j^2\right), \end{aligned} \quad (6)$$

where N_τ is the number of neutrons or protons in a nucleus and $\sum^\tau$ implies a summation over neutron or proton single-particle states only. From the numerical solution of Eqs. (6) it is found that the (pseudo-)critical temperature is $T_{\text{cr}} \approx \frac{1}{2} \Delta_\tau(0)$ (see, e.g., Refs. [32] and [33]), in accordance with the BCS theory.

With the coefficients u_j, v_j, x_j, and y_j, defined by Eqs. (4) and (5), the one-body part of $\mathcal{H}_{\text{sp}} + \mathcal{H}_{\text{pair}}$ reads

$$\mathcal{H}_{\text{sp}} + \mathcal{H}_{\text{pair}} \simeq \sum_\tau \sum_{jm}^\tau \varepsilon_j (\beta^\dagger_{jm} \beta_{jm} - \widetilde{\beta}^\dagger_{jm} \widetilde{\beta}_{jm}) \quad (7)$$

and corresponds to a system of noninteracting thermal quasi-particles. The vacuum for thermal quasiparticles (hereafter denoted $|0(T); \text{qp}\rangle$) is the thermal vacuum in the BCS approximation. The states $\beta^\dagger_{jm}|0(T); \text{qp}\rangle$ have positive excitation energies, whereas the corresponding tilde states $\widetilde{\beta}^\dagger_{jm}|0(T); \text{qp}\rangle$ have negative energies.

The coefficients y_j^2 defined through Eq. (5) determine the average number of thermally excited Bogoliubov quasiparticles in the BCS thermal vacuum,

$$\langle 0(T); \text{qp}|\alpha^\dagger_{jm} \alpha_{jm}|0(T); \text{qp}\rangle = y_j^2 \quad (8)$$

and, thus, coincide with the thermal occupation factors of the Fermi-Dirac statistics. Because the thermal vacuum $|0(T); \text{qp}\rangle$ contains a certain number of Bogoliubov quasiparticles, excited states can be built on $|0(T); \text{qp}\rangle$ by either adding or removing a Bogoliubov quasiparticle. Because

$$\begin{aligned} \alpha^\dagger_{jm}|0(T); \text{qp}\rangle &= x_j \beta^\dagger_{jm}|0(T); \text{qp}\rangle, \\ \alpha_{\overline{jm}}|0(T); \text{qp}\rangle &= -i y_j \widetilde{\beta}^\dagger_{jm}|0(T); \text{qp}\rangle \\ [\alpha_{\overline{jm}} &= (-1)^{j-m} \alpha_{j-m}], \end{aligned} \quad (9)$$

the first process corresponds to the creation of a nontilde thermal quasiparticle with positive energy, whereas the second process creates a tilde quasiparticle with negative energy.

In the next step of the approximate diagonalization of $\mathcal{H}_{\text{QPM}}$, long-range correlations owing to the particle-hole interaction are taken into account within the proton-neutron TQRPA. The part of $\mathcal{H}_{\text{ph}}$ in Eq. (2) responsible for charge-

exchange excitations reads

$$\mathcal{H}_{\text{ph}}^{\text{ch}} = -2 \sum_{\lambda\mu} \kappa_1^{(\lambda)} (M_{\lambda\mu}^\dagger M_{\lambda\mu} - \widetilde{M}_{\lambda\mu}^\dagger \widetilde{M}_{\lambda\mu})$$
$$- 2 \sum_{L\lambda\mu} \kappa_1^{(L\lambda)} (S_{L\lambda\mu}^\dagger S_{L\lambda\mu} - \widetilde{S}_{L\lambda\mu}^\dagger \widetilde{S}_{L\lambda\mu}), \quad (10)$$

where $M_{\lambda\mu}^\dagger$ and $S_{L\lambda\mu}^\dagger$ are single-particle multipole and spin-multipole operators:

$$M_{\lambda\mu}^\dagger = \sum_{\substack{j_p m_p \\ j_n m_n}} \langle j_p m_p | i^\lambda r^\lambda Y_{\lambda\mu}(\theta,\phi) t^{(-)} | j_n m_n \rangle a_{j_p m_p}^\dagger a_{j_n m_n},$$

$$S_{L\lambda\mu}^\dagger = \sum_{\substack{j_p m_p \\ j_n m_n}} \langle j_p m_p | i^L r^L [Y_L \sigma]_\mu^\lambda t^{(-)} | j_n m_n \rangle a_{j_p m_p}^\dagger a_{j_n m_n},$$

$$[Y_L \sigma]_\mu^\lambda = \sum_{M,m} \langle LM1m|\lambda\mu\rangle Y_{LM}(\theta,\phi)\sigma_m. \quad (11)$$

The parameters $\kappa_1^{(\lambda)}$ and $\kappa_1^{(L\lambda)}$ denote the strength parameters of the isovector multipole and spin-multipole forces, respectively. The states of natural parity are generated by the multipole and spin-multipole $L = \lambda$ interactions, whereas the spin-multipole interactions with $L = \lambda \pm 1$ are responsible for the states of unnatural parity.

Within the TFD formalism the TQRPA equations are derived in the following way. First, $\mathcal{H}_{\text{ph}}^{\text{ch}}$ is written in terms of the thermal quasiparticle operators. Then the sum of Eq. (7) and $\mathcal{H}_{\text{ph}}^{\text{ch}}$ is diagonalized with respect to charge-exchange thermal phonons.

The thermal phonon creation operator $Q_{\lambda\mu i}^\dagger$ is defined as a linear superposition of the proton-neutron thermal two-quasiparticle operators,

$$Q_{\lambda\mu i}^\dagger = \sum_{j_p j_n} \left(\psi_{j_p j_n}^{\lambda i} [\beta_{j_p}^\dagger \beta_{j_n}^\dagger]_\mu^\lambda + \widetilde{\psi}_{j_p j_n}^{\lambda i} [\widetilde{\beta}_{\overline{j_p}}^\dagger \widetilde{\beta}_{\overline{j_n}}^\dagger]_\mu^\lambda \right.$$
$$+ i\eta_{j_p j_n}^{\lambda i} [\beta_{j_p}^\dagger \widetilde{\beta}_{\overline{j_n}}^\dagger]_\mu^\lambda + i\widetilde{\eta}_{j_p j_n}^{\lambda i} [\widetilde{\beta}_{\overline{j_p}}^\dagger \beta_{j_n}^\dagger]_\mu^\lambda$$
$$+ \phi_{j_p j_n}^{\lambda i} [\beta_{\overline{j_p}} \beta_{\overline{j_n}}]_\mu^\lambda + \widetilde{\phi}_{j_p j_n}^{\lambda i} [\widetilde{\beta}_{j_p} \widetilde{\beta}_{j_n}]_\mu^\lambda$$
$$\left. + i\xi_{j_p j_n}^{\lambda i} [\beta_{\overline{j_p}} \widetilde{\beta}_{j_n}]_\mu^\lambda + i\widetilde{\xi}_{j_p j_n}^{\lambda i} [\widetilde{\beta}_{j_p} \beta_{\overline{j_n}}]_\mu^\lambda \right), \quad (12)$$

where $[\ ]_\mu^\lambda$ denotes the coupling of single-particle angular momenta j_n, j_p to the total angular momentum λ. Now the thermal equilibrium state is treated as the vacuum $|0(T);\text{ph}\rangle$ for thermal phonon annihilation operators.

The thermal phonon operators are assumed to commute as bosonic operators, that is, $[Q_{\lambda\mu i}, Q_{\lambda'\mu'i'}^\dagger] = \delta_{\lambda\lambda'}\delta_{\mu\mu'}\delta_{ii'}$. This assumption imposes the following constraint on the phonon amplitudes:

$$\sum_{j_p j_n} \left(\psi_{j_p j_n}^{\lambda i} \psi_{j_p j_n}^{\lambda i'} + \widetilde{\psi}_{j_p j_n}^{\lambda i} \widetilde{\psi}_{j_p j_n}^{\lambda i'} + \eta_{j_p j_n}^{\lambda i} \eta_{j_p j_n}^{\lambda i'} \right.$$
$$+ \widetilde{\eta}_{j_p j_n}^{\lambda i} \widetilde{\eta}_{j_p j_n}^{\lambda i'} - \phi_{j_p j_n}^{\lambda i} \phi_{j_p j_n}^{\lambda i'} - \widetilde{\phi}_{j_p j_n}^{\lambda i} \widetilde{\phi}_{j_p j_n}^{\lambda i'}$$
$$\left. - \xi_{j_p j_n}^{\lambda i} \xi_{j_p j_n}^{\lambda i'} - \widetilde{\xi}_{j_p j_n}^{\lambda i} \widetilde{\xi}_{j_p j_n}^{\lambda i'} \right) = \delta_{ii'}. \quad (13)$$

Furthermore, the phonon amplitudes obey the closure relation.

Demanding that the vacuum of thermal phonons obeys the thermal-state condition (1) and applying the variational prin-

ciple to the average value of the thermal Hamiltonian with respect to one-phonon states $Q_{\lambda\mu i}^\dagger|0(T);\text{ph}\rangle$ or $\widetilde{Q}_{\lambda\mu i}^\dagger|0(T);\text{ph}\rangle$[1] under the constraints (13), one gets a system of linear equations for the amplitudes $\psi_{j_p j_n}^{\lambda i}$, $\widetilde{\psi}_{j_p j_n}^{\lambda i}$, $\eta_{j_p j_n}^{\lambda i}$, $\widetilde{\eta}_{j_p j_n}^{\lambda i}$, etc. The system has a nontrivial solution if the energy $\omega_{\lambda i}$ of the thermal one-phonon state obeys the following secular equation:

$$\begin{vmatrix} X_{aa}^{(+)} - \dfrac{1}{\kappa_1^{(a)}} & X_{aa}^{(+-)} & X_{ab}^{(+)} & X_{ab}^{(+-)} \\[1.5em] X_{aa}^{(-+)} & X_{aa}^{(-)} - \dfrac{1}{\kappa_1^{(a)}} & X_{ab}^{(-+)} & X_{ab}^{(-)} \\[1.5em] X_{ab}^{(+)} & X_{ab}^{(+-)} & X_{bb}^{(+)} - \dfrac{1}{\kappa_1^{(b)}} & X_{bb}^{(+-)} \\[1.5em] X_{ab}^{(+-)} & X_{ab}^{(-)} & X_{ab}^{(-+)} & X_{bb}^{(-)} - \dfrac{1}{\kappa_1^{(b)}} \end{vmatrix} = 0,$$

$$(14)$$

where $a \equiv \lambda$ and $b \equiv \lambda\lambda$ for excitations of natural parity, whereas $a \equiv (\lambda-1)\lambda$ and $b \equiv (\lambda+1)\lambda$ for unnatural-parity excitations. The functions $X_{cd}^{(\pm)}$, $X_{cd}^{(\pm\mp)}$ ($c = a, b$ and $d = a, b$) in Eq. (14) are defined as

$$X_{cd}^{(\pm)}(\omega) = \frac{2}{\hat{\lambda}^2} \sum_{j_p j_n} f_{j_p j_n}^{(c)} f_{j_p j_n}^{(d)} \left\{ \frac{\varepsilon_{j_p j_n}^{(+)} [u_{j_p j_n}^{(\pm)}]^2}{[\varepsilon_{j_p j_n}^{(+)}]^2 - \omega^2} \right.$$
$$\left. \times (1 - y_{j_p}^2 - y_{j_n}^2) - \frac{\varepsilon_{j_p j_n}^{(-)} [v_{j_p j_n}^{(\mp)}]^2}{[\varepsilon_{j_p j_n}^{(-)}]^2 - \omega^2} (y_{j_p}^2 - y_{j_n}^2) \right\},$$

$$X_{cd}^{(\pm\mp)}(\omega) = \frac{2\omega}{\hat{\lambda}^2} \sum_{j_p j_n} f_{j_p j_n}^{(c)} f_{j_p j_n}^{(d)} \left\{ \frac{u_{j_p j_n}^{(\pm)} u_{j_p j_n}^{(\mp)}}{[\varepsilon_{j_p j_n}^{(+)}]^2 - \omega^2} \right.$$
$$\left. \times (1 - y_{j_p}^2 - y_{j_n}^2) - \frac{v_{j_p j_n}^{(\pm)} v_{j_p j_n}^{(\mp)}}{[\varepsilon_{j_p j_n}^{(-)}]^2 - \omega^2} (y_{j_p}^2 - y_{j_n}^2) \right\}.$$

$$(15)$$

Here $f_{j_p j_n}^{(\lambda)}$ and $f_{j_p j_n}^{(L\lambda)}$ denote the reduced single-particle matrix elements of the multipole and spin-multipole operators, Eq. (11); $u_{j_p j_n}^{(\pm)} = u_{j_p} v_{j_n} \pm v_{j_p} u_{j_n}$ and $v_{j_p j_n}^{(\pm)} = u_{j_p} u_{j_n} \pm v_{j_p} v_{j_n}$; $\varepsilon_{j_p j_n}^{(\pm)} = \varepsilon_{j_p} \pm \varepsilon_{j_n}$; and $\hat{\lambda} = \sqrt{2\lambda+1}$.

Let us consider the secular equation in detail. The poles $\varepsilon_{j_p j_n}^{(-)}$, which do not exist in the QRPA equations at zero temperature, arise from the crossed terms $\beta^\dagger\widetilde{\beta}^\dagger$ in the thermal phonon operator definition, Eq. (12). Because of these poles, new states appear in a low-energy part of the thermal excitation spectrum. In contrast to the zero-temperature case, the negative solutions of the secular equation now have a physical meaning. They correspond to the tilde thermal one-phonon states and arise from $\widetilde{\beta}^\dagger\widetilde{\beta}^\dagger$ terms in the thermal phonon operator.

---

[1]We take into account that the operator $\widetilde{Q}_{\lambda\mu i}^\dagger = (-1)^{\lambda-\mu}\widetilde{Q}_{\lambda-\mu i}^\dagger$ transforms under spatial rotations like a spherical tensor of rank λ.

As noted previously, the creation of a tilde thermal quasiparticle corresponds to the annihilation of a thermally excited Bogoliubov quasiparticle. Consequently, excitations of low- and negative-energy thermal phonons correspond to transitions from thermally excited nuclear states. Furthermore, when the pairing correlations vanish (i.e., $T > T_{\rm cr}$), some poles no longer contribute to the secular equation, as the corresponding numerators vanish. This is true for particle-particle and hole-hole $\varepsilon_{j_p j_n}^{(+)}$ poles as well as for particle-hole $\varepsilon_{j_p j_n}^{(-)}$ poles.

The expressions for the thermal charge-exchange phonon amplitudes are given in Ref. [28]. The amplitudes depend on both the quasiparticle and the phonon thermal occupation numbers. Some remarks are in order. TQRPA equations for GT excitations at finite temperature were also derived in Ref. [34]. They were obtained using the equation of motion method by replacing vacuum expectation values with thermal averages, that is, without applying the TFD formalism and doubling the Hilbert space. Therefore, in contrast with the present study, negative solutions of the TQRPA equations were neglected in Ref. [34].

After diagonalization within the TQRPA the thermal Hamiltonian $\mathcal{H}_{\rm QPM}$ becomes

$$\mathcal{H}_{\rm QPM} = \sum_{\lambda \mu i} \omega_{\lambda i} (Q_{\lambda \mu i}^{\dagger} Q_{\lambda \mu i} - \widetilde{Q}_{\lambda \mu i}^{\dagger} \widetilde{Q}_{\lambda \mu i}). \quad (16)$$

The vacuum $|0(T); {\rm ph}\rangle$ of thermal phonons is the thermal vacuum in the TQRPA. Because we use the thermal BCS approximation, which violates the particle number, the charge-exchange thermal one-phonon states are superpositions of states, which belong to the daughter nuclei $(N - 1, Z + 1)$ and $(N + 1, Z - 1)$. They decouple at temperatures $T \geqslant T_{\rm cr}$, when the pairing correlations vanish. Then, if the state $Q_{\lambda \mu i}^{\dagger} |0(T); {\rm ph}\rangle$ belongs to the $(N \pm 1, Z \mp 1)$ nucleus, the state $\widetilde{Q}_{\lambda \mu i}^{\dagger} |0(T); {\rm ph}\rangle$ is in the $(N \mp 1, Z \pm 1)$ nucleus.

III. ELECTRON CAPTURE RATES

Considering EC in stellar environments we make the following assumptions. (1) The temperature in the stellar interior is so high that atoms are fully ionized, and the surrounding electron gas is described by a Fermi-Dirac distribution, with temperature T and chemical potential μ_e. Neutrinos escape freely from the interior of the star. Hence no Pauli blocking for neutrinos is considered in the final state. (2) The parent nucleus is in a thermal equilibrium state treated as the thermal (phonon) vacuum. (3) EC leads to charge-exchange transitions from the thermal vacuum to thermal one-phonon states.

In these circumstances the EC rate is the sum of the transition rates from the thermal vacuum to the ith thermal one-phonon state of the multipolarity J,

$$\lambda^{\rm ec} = \frac{\ln 2}{6150 \text{ s}} \sum_J \sum_i \Phi_{Ji}^{(+)} F_i^{\rm ec} = \sum_J \sum_i \lambda_{Ji}^{\rm ec}. \quad (17)$$

Here $\Phi_{Ji}^{(+)}$ is the squared reduced matrix element of the transition operator between the thermal phonon vacuum and a thermal one-phonon state (see the following); $F_i^{\rm ec}$ is a phase-space factor that depends on the transition energy $E_{Ji}^{(+)}$ and can be found elsewhere [9].

Denoting the proton-to-neutron $(p \to n)$ transition operator with multipolarity J as $D_J^{(+)}$, one obtains the following expression for the transition strength $\Phi_{Ji}^{(+)}$:

$$\Phi_{Ji}^{(+)} = \left| \langle 0(T); {\rm ph} \| Q_{JMi} D_J^{(+)} \| 0(T); {\rm ph} \rangle \right|^2$$
$$= \left[\sum_{j_p j_n} (-1)^{j_n - j_p + J} d_J^{(+)}(j_p j_n) \Omega(j_p j_n; Ji) \right]^2, \quad (18)$$

where $d_J^{(+)}(j_p j_n) = \langle j_n \| D_J^{(+)} \| j_p \rangle$ is a reduced single-particle matrix element of the transition operator, and the function $\Omega(j_p j_n; Ji)$ is given by

$$\Omega(j_p j_n; Ji) = v_{j_p} u_{j_n} \left(x_{j_p} x_{j_n} \psi_{j_p j_n}^{Ji} + y_{j_p} y_{j_n} \widetilde{\phi}_{j_p j_n}^{Ji} \right)$$
$$+ u_{j_p} v_{j_n} \left(y_{j_p} y_{j_n} \widetilde{\psi}_{j_p j_n}^{Ji} + x_{j_p} x_{j_n} \phi_{j_p j_n}^{Ji} \right)$$
$$- v_{j_p} v_{j_n} \left(x_{j_p} y_{j_n} \eta_{j_p j_n}^{Ji} + y_{j_p} x_{j_n} \widetilde{\xi}_{j_p j_n}^{Ji} \right)$$
$$+ u_{j_p} u_{j_n} \left(y_{j_p} x_{j_n} \widetilde{\eta}_{j_p j_n}^{Ji} + x_{j_p} y_{j_n} \xi_{j_p j_n}^{Ji} \right). \quad (19)$$

The transition strength to the tilde one-phonon state can be easily obtained from Eqs. (18) and (19) by changing nontilde phonon amplitudes by their tilde counterparts, and vice versa. (The expressions for the transition strengths $\Phi_{Ji}^{(-)}$ corresponding to inverse $n \to p$ transitions are given in Ref. [28]. It has been proved in Ref. [28] that the approach used here fulfills the Ikeda sum rule for Fermi and GT transitions.)

The transition energy (parent excitation energy) $E_{Ji}^{(+)}$ can be obtained from the energy shift between the proton subsystem of the parent nucleus and the neutron subsystem of the daughter nucleus including the proton-neutron mass difference. Thus we have

$$E_{Ji}^{(+)} = \omega_{Ji} + (\Delta \mu_{np} + \Delta m_{np}), \quad (20)$$

where $\Delta \mu_{np} = \mu_p - \mu_n$ is the difference between the neutron and the proton chemical potentials and $\Delta m_{np} = m_n - m_p$ is the neutron-proton mass splitting. Note that at finite temperature the energies $E_{Ji}^{(+)}$ as well as ω_{Ji} can be both positive and negative. Thus, for the capture process thermal one-phonon states with both positive and negative values of $E_{Ji}^{(+)}$ contribute to the rate.

In what follows in Eq. (17) we take into account the contributions from allowed (GT and Fermi) transitions and FF transitions. The operators of allowed Fermi and GT transitions are taken in the standard form,

$$D_{0^+}^{(+)} = g_V t^{(+)}, \quad D_{1^+}^{(+)} = g_A \boldsymbol{\sigma} t^{(+)}, \quad (21)$$

where $t^{(+)}$ is the isospin raising operator. For the operators of the FF $n \to p$ transitions the nonrelativistic form is used:

$$D_{0^-}^{(+)} = g_A \left[\frac{\boldsymbol{\sigma} \cdot \boldsymbol{p}}{m} + \frac{\alpha Z}{2R} i \boldsymbol{\sigma} \cdot \boldsymbol{r} \right] t^{(+)},$$
$$D_{1^-}^{(+)} = \left[g_V \frac{\boldsymbol{p}}{m} - \frac{\alpha Z}{2R} (g_A \boldsymbol{\sigma} \times \boldsymbol{r} - i g_V \boldsymbol{r}) \right] t^{(+)}, \quad (22)$$
$$D_{2^-}^{(+)} = i \frac{g_A}{\sqrt{3}} [\boldsymbol{\sigma} \cdot \boldsymbol{r}]_{\mu}^2 \sqrt{p_e^2 + q_{\nu}^2} t^{(+)}.$$

In Eqs. (21) and (22), $\boldsymbol{r}$, $\boldsymbol{p}$, and $\boldsymbol{\sigma}$ refer to the coordinate, momentum, and spin operators of a nucleon; $g_V = 1$ and $g_A = -1.25$ denote the vector and axial coupling constants; α is the

fine structure constant; Z and R are the charge and the radius of the nucleus; m is the nucleon mass; and p_e and q_ν denote the momenta of the incoming electron and outgoing neutrino, respectively.

IV. IRON ISOTOPES

In this section we discuss the numerical results for the pf-shell nuclei ^{54,56}Fe. Experimental data are available for these nuclei to test our calculations at zero temperature. Moreover, these iron isotopes are among the most essential nuclei in their importance to the EC process for the early presupernova collapse [6,35].

The proton and neutron mean fields are described by spherically symmetric Woods-Saxon potentials with parameters from Ref. [36]. We only readjust the potential depths to fit the proton and neutron binding energies of the parent nucleus to their experimental values. The single-particle basis includes all discrete bound states as well as selected quasibound states with large j in the continuum. The proton (neutron) pairing strength parameters $G_{p(n)}$ are fixed to reproduce the odd-even mass difference through a four-term formula [37] involving the experimental binding energies [38]. At $T = 0$ the obtained proton and neutron BCS energy gaps are $\Delta_{p(n)} = 1.52(0.0)$ MeV for ^{54}Fe[2] and $\Delta_{p(n)} = 1.57(1.36)$ MeV for ^{56}Fe. The isovector strength parameters $\kappa_1^{(01)}$ and $\kappa_1^{(21)}$ are adjusted to reproduce the experimental centroid energies of the GT$_-$ and GT$_+$ resonances in the nuclei under consideration [39–41]. The corresponding values of $\kappa_1^{(01)}$ and $k_1^{(21)}$ are in agreement with the rough estimates in Ref. [42]. The spin-quadrupole interaction weakly affects the GT strength distributions.

The total GT strengths calculated with the bare GT$_\pm$ operators $\sigma t^{(\pm)}$ are $S_+ = 6.6$ and $S_- = 12.7$ in ^{54}Fe and $S_+ = 5.1$ and $S_- = 17.0$ in ^{56}Fe, respectively. These $S_\mp$ values obey the Ikeda sum rule (a small deviation is caused by the incompleteness of our single-particle basis) but noticeably overestimate experimental data (see, e.g., Refs. [39–41]). This is common for any RPA [or quasiparticle RPA (QRPA)] calculation of GT strength and is remedied by an effective value for the axial weak coupling constant. We use $g_A^* = 0.74 g_A$ as in shell-model calculations [9].

In Fig. 1, the experimental and theoretical (quenched) distributions of GT$_+$ strengths are presented. There we also compare the GT$_+$ running sums corresponding to the experimental, QRPA, and large-scale shell-model (LSSM) [9] strength distributions. One can see that the QRPA calculations reproduce the resonance positions but not the fragmentation of the strength. It is a well-known fact that RPA calculations cannot describe the full resonance width (at least in spherical nuclei) and produce only a part of it, the so-called Landau width. The latter is quite small for the GT resonance. As a result, the near-threshold part of the GT$_+$ strength, which corresponds to transitions to low-lying 1^+ states in the daughter
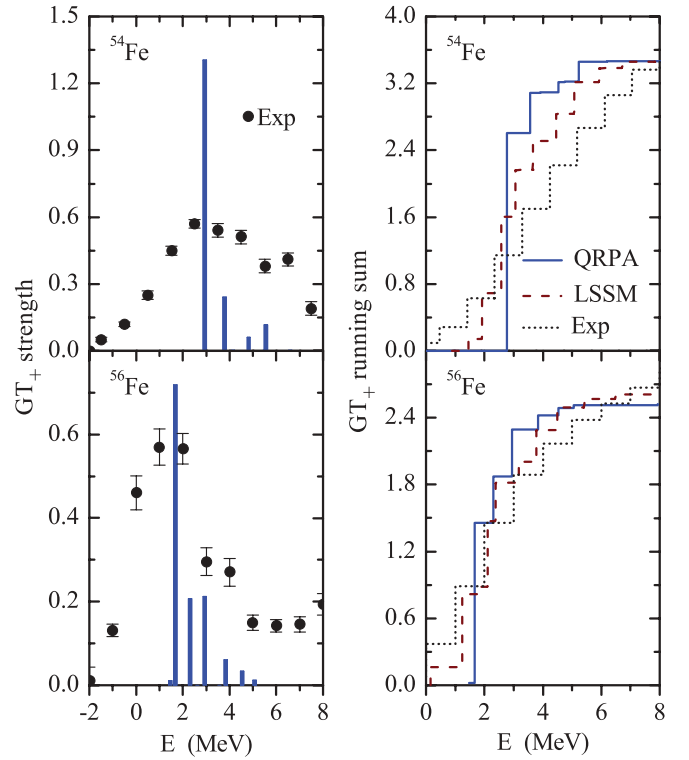
---

^{2} ^{54}Fe has a closed $1f_{7/2}$ neutron subshell in our single-particle scheme.

FIG. 1. (Color online) Left panels: Comparison of GT$_+$ experimental data [40,41] with the calculated QRPA strength distributions for ^{54,56}Fe. The QRPA peaks are scaled by 0.5 for convenience. Right panels: Comparison of the GT$_+$ running sums corresponding to the experimental, QRPA, and LSSM [9] strength distributions.

nuclei ^{54,56}Mn, is not reproduced in our calculations. In this respect shell-model calculations are clearly advantageous.

We now turn to the temperature evolution of the GT$_+$ strength distributions. The strength distributions for ^{54,56}Fe at several temperatures are shown in Fig. 2. All figures are plotted as a function of the energy transfer E to the parent nucleus.

With increasing temperature, in our model, two effects occur that influence the GT$_+$ strength distribution.

(i) At low temperatures, owing to pairing, GT$_+$ transitions involve the breaking of a proton Cooper pair associated with some energy cost. This extra energy is removed at $T > T_{\rm cr}$ ($T_{\rm cr} \approx 0.8$ MeV) and the peak in the GT$_+$ distribution moves to lower energies. Some extra energy has to be paid at low temperatures to add one more nucleon to the neutron subsystem of ^{56}Fe because of the nonzero neutron energy gap. Obviously, this energy is also removed at $T > T_{\rm cr}$.

(ii) GT$_+$ transitions, which are Pauli blocked at low temperatures owing to closed neutron subshells (e.g., $1f_{7/2}$ orbital), become thermally unblocked with increasing temperature. Similarly, protons that are thermally excited to higher orbitals can undergo GT$_+$ transitions. In TFD such transitions are taken into account by $\beta_{j_p}^\dagger \widetilde{\beta}_{\bar{j}_n}^\dagger$, $\widetilde{\beta}_{\bar{j}_p}^\dagger \beta_{j_n}^\dagger$, and $\widetilde{\beta}_{\bar{j}_p}^\dagger \widetilde{\beta}_{\bar{j}_n}^\dagger$ components of the thermal phonon. Because of thermally unblocked transitions, some GT$_+$
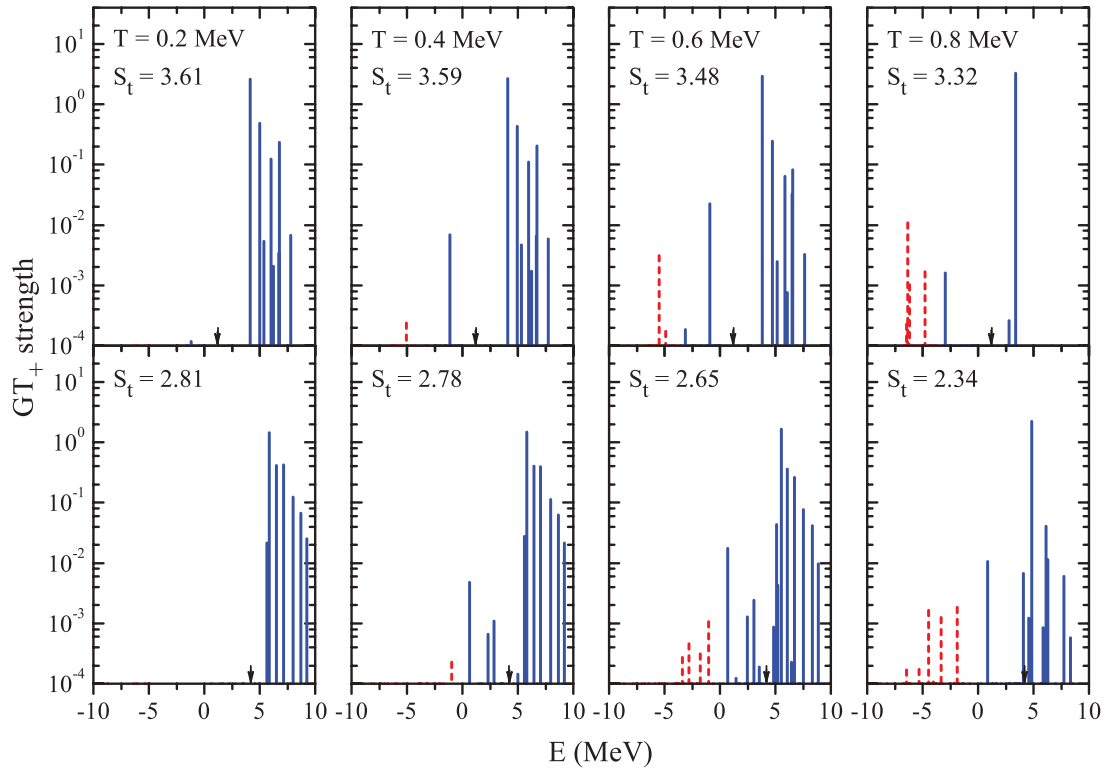
FIG. 2. (Color online) Temperature evolution of GT_+ strength distributions for ^{54}Fe (upper panels) and for ^{56}Fe (lower panels) versus parent excitation energy. The solid (dashed) lines refer to transitions to nontilde (tilde) thermal one-phonon states. S_t is the total GT_+ strength. The arrows indicate the zero-temperature threshold $Q = M_f - M_i$, where $M_{i,f}$ are the masses of the parent and daughter nuclei. $Q(^{54}\text{Fe}) = 1.21$ MeV and $Q(^{56}\text{Fe}) = 4.20$ MeV.

strength appears well below the zero-temperature threshold, including negative energies.

Owing to the vanishing of the pairing correlations and the appearance of negative- and low-energy transitions, the centroids of the GT_+ strength distributions in ^{54,56}Fe are shifted to lower excitation energies at high temperatures. Our calculations indicate that a temperature increase to 0.8 MeV results in GT_+ centroid shifts of the order of 1.5 MeV for ^{54}Fe and 2.5 MeV for ^{56}Fe. Thus the present approach violates Brink's hypothesis. Similar results have been obtained in SMMC calculations of GT centroids at finite temperatures. We also observe (see Fig. 2) a gradual decrease in the total GT_+ strength when the temperature increases from 0 to 0.8 MeV. Nevertheless, as pointed out previously, the present approach preserves the Ikeda sum rule at finite temperatures.

The calculated GT_+ strength distributions were used to obtain the stellar EC rates for ^{54,56}Fe. The rates were calculated for densities between $\log_{10}(\rho Y_e) = 7$ and $\log_{10}(\rho Y_e) = 10$ as a function of temperature T_9 ($T_9 = 10^9$ K and 1 MeV $\approx 11.6 T_9$). A comparison between the TQRPA rates and the LSSM results [10] is presented in Fig. 3.

As must be, the EC rates increase with temperature and density. Owing to the larger value of the zero-temperature threshold Q for ^{56}Fe, both approaches yield a higher rate for ^{54}Fe than for ^{56}Fe at a given temperature and density. Both approaches give very similar values for the strength and the location of the GT_+ resonance in ^{54,56}Fe at $T = 0$. Therefore,

the excellent agreement between the TQRPA and the shell-model rates at $\log_{10}(\rho Y_e) = 10$ and low temperatures ($\mu_e \approx 11$ MeV) is not surprising, as the rates are dominated by the resonance contribution.

The more interesting point is that at high temperatures the TQRPA rates always surpass the shell-model ones. To understand this point, which part of the TQRPA GT_+ strength dominates EC at a given temperature and density must be clarified. To this end we calculate the relative contributions $\lambda_i^{\text{ec}}/\lambda^{\text{ec}}$ of different thermal one-phonon states to the capture rates for selected values of temperature and density $[T_9, \log_{10}(\rho Y_e)]$. The results are depicted in Fig. 4.

At low temperatures and densities [Figs. 4(a) and 4(b)], that is, when μ_e is small and high-energy electrons from the tail of the Fermi-Dirac distribution are not sufficiently available to allow for efficient capture on the GT_+ resonance, the TQRPA capture rates are dominated either by the negative-energy (^{54}Fe) or by the low-energy (^{56}Fe) part of the GT_+ strength that originates from thermally unblocked $p \rightarrow n$ transitions. The TQRPA rates are larger than those of the shell model at low (T, ρ) owing to differences in the strength and the energy of such transitions. We note that in the shell-model evaluation, negative-energy transitions were mainly included by back-resonances, that is, by inverting the Fermi and GT_- strength distribution of ^{54}Mn and ^{56}Mn, respectively. In contrast to the TQRPA approach, the shell-model GT_- distributions of these nuclei are highly fragmented owing
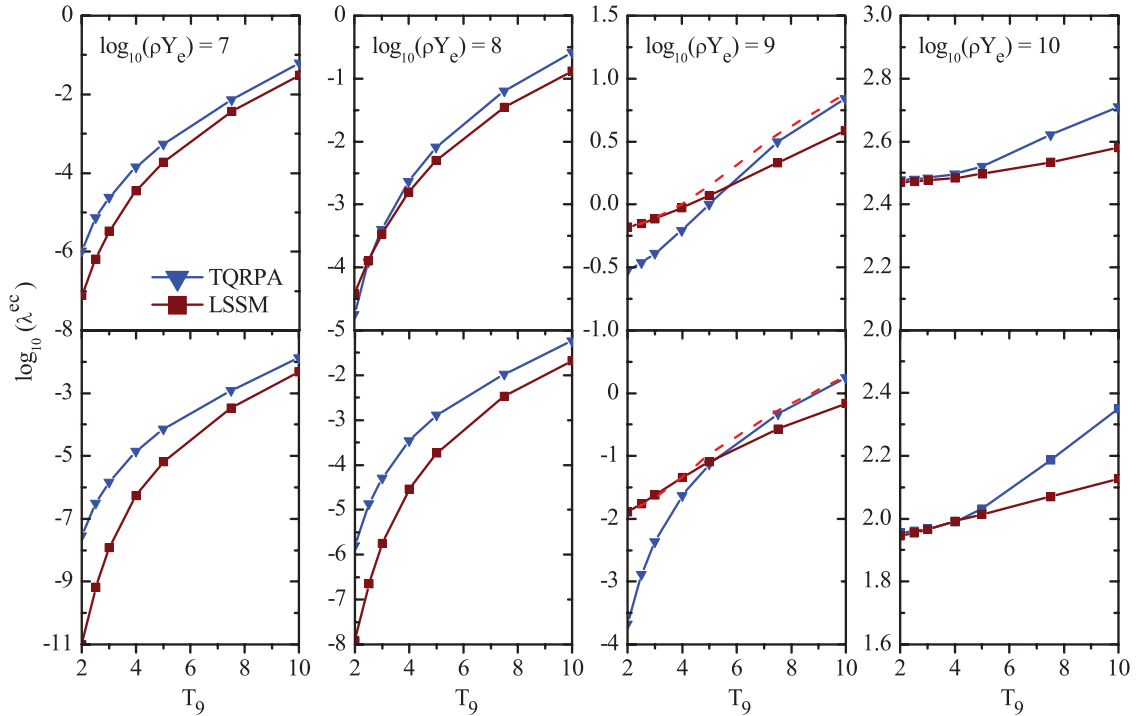
FIG. 3. (Color online) Electron capture rates for ^{54}Fe (upper panels) and ^{56}Fe (lower panels) calculated using the TQRPA approach as a function of temperature (T_9 measures the temperature in 10^9 K) and for selected values of density ρY_e (g cm^{-3}). For comparison, the LSSM rates [10] are also shown. The dashed lines at $\log_{10}(\rho Y_e) = 9$ correspond to the TQRPA rates calculated with the assigned near-threshold strength (see text).

to correlations and have centroids at rather high excitation energies in ^{54}Fe and ^{56}Fe, which, at low temperatures, are strongly suppressed by the Boltzmann factor. In particular, the differences in energy positions of the transitions are important because at low (T, ρ) the rates can change drastically upon a small change in a transition energy. To see whether the TQRPA reliably predicts the energy and the strength of negative- and low-energy transitions, one must go beyond the TQRPA.

At $\log_{10}(\rho Y_e) = 9$ and $T_9 < 5$ ($\mu_e \approx 5.1$ MeV), the near-threshold part of the GT$_+$ strength dominates the capture rates. Because this part is not reproduced within the TQRPA, the rates appear to be lower than the LSSM ones. To test this hypothesis, the capture rates at $\log_{10}(\rho Y_e) = 9$ have been calculated— guided by the shell-model GT$_+$ distributions [9]—assuming that the near-threshold GT$_+$ strengths for ^{54}Fe and ^{56}Fe are 0.1 and 0.2, respectively. We therefore assign the value 0.1 (0.2) to the GT$_+$ strength in ^{54}Fe (^{56}Fe) at the zero-temperature threshold. (A similar method was used in Refs. [5] and [6] to include the contribution of low-lying transitions.) This yields a much better agreement between the TQRPA and the shell-model rates (see Fig. 3). Thus, to improve the reliability of the TQRPA for the calculation of stellar EC rates at intermediate densities and low temperatures, the fragmentation of the GT$_+$ resonance should be considered to reproduce the near-threshold GT$_+$ strength. At higher temperatures the near-threshold strength becomes less important. In Figs. 4(c) and 4(d) the relative contributions $\lambda_i^{ec}/\lambda^{ec}$ at $[T_9, \log_{10}(\rho Y_e)] =$

(5, 9) with and without the assigned near-threshold strength are depicted. As can be seen, the contribution from the near-threshold strength is not dominant.

When the temperature approaches $T_9 \approx 10$, the rates are dominated by the strong transitions involving the GT$_+$ resonance at low [Fig. 4(e)] as well as at high [Fig. 4(f)] densities. [Note that at $\log_{10}(\rho Y_e) = 7$ and high temperatures the contribution of negative-energy transitions is non-negligible.] As discussed previously, the TQRPA predicts that with increasing temperature the GT$_+$ resonance shifts to lower excitation energies. This explains why the TQRPA rates always surpass the LSSM ones at high temperatures.

Thus, at high densities and low temperatures the TQRPA and LSSM EC rates for ^{54,56}Fe are in good agreement. As mentioned previously the disagreement at moderate densities and low temperatures can be removed by considering the fragmentation of the GT$_+$ strength. For a separable residual interaction used here this can be done following the method developed within the QPM, that is, by taking phonon coupling into account.

V. NEUTRON-RICH GERMANIUM ISOTOPES

During gravitational collapse the nuclear composition moves toward a higher mass number and more neutron-rich nuclei. Eventually nuclei will have all neutron pf-shell orbits filled, with valence neutrons in the sdg shell ($N > 40$)
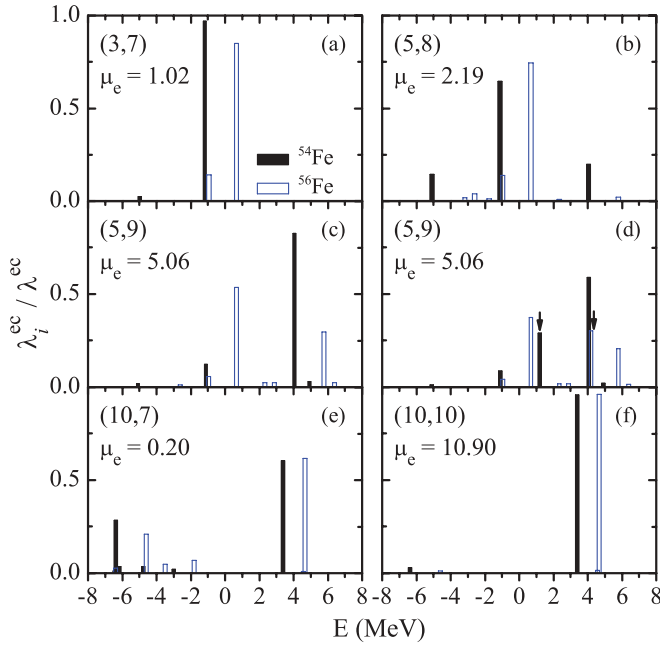
FIG. 4. (Color online) Relative contribution $\lambda_i^{ec}/\lambda^{ec}$ of the ith thermal one-phonon state to the EC rate on ^{54,56}Fe for selected values of temperature and density [T_9, $\log_{10}(\rho Y_e)$]. The electron chemical potential μ_e is in units of mega–electron volts; E is the transition energy to the ith thermal one-phonon state. The arrows in (d) indicate the relative contributions of the assigned near-threshold strengths (see text).

FIG. 5. (Color online) Strength distribution (folded) of allowed (0^+ and 1^+) $p \rightarrow n$ transitions in ^{76}Ge at various temperatures T. E denotes the transition energy. The contribution of 0^+ transitions is shown by the dashed line. S_t is the total strength. The arrows indicate the zero-temperature threshold $Q(^{76}$Ge$) = M_f - M_i = 7.52$ MeV. A and B label the transitions: $A \equiv 1f_{7/2}^p \rightarrow 1f_{5/2}^n$, $B \equiv 1g_{9/2}^p \rightarrow 1g_{7/2}^n$.

and valence protons within the pf shell ($Z < 40$). The Pauli principle blocks GT$_+$ transitions in such neutron-rich nuclei if the independent particle model is used. It has been demonstrated in Ref. [4] that, at high enough temperatures, $T \sim 1.5$ MeV, GT$_+$ transitions become unblocked by thermal excitations that either move protons into the $1g_{9/2}$ orbital or remove neutrons from the pf shell. An alternative unblocking mechanism—configuration mixing induced by the residual interaction—was considered in Ref. [20]. Based on this approach it was found that EC on nuclei with $N > 40$ is also dominated by GT$_+$ transitions, even at rather low stellar temperatures, $T \sim 0.5$ MeV. Contrary to Ref. [4], it was argued that unblocking effects owing to mixing are not very sensitive to increasing temperature.

Consistent calculations of EC rates for neutron-rich nuclei are not yet feasible in the shell model owing to the large model space. In Ref. [20], the capture rates were calculated adopting a hybrid model: The partial occupation numbers calculated within the SMMC approach at finite temperature were used in calculations based on the RPA. Here, using the germanium isotopes ^{76,78,80}Ge as examples, we apply the TQRPA formalism to calculate EC rates on neutron-rich nuclei. Particular attention is paid to the temperature dependence of the unblocking effect.

The parameters of the model Hamiltonian for ^{76,78,80}Ge are chosen in the same manner as for ^{54,56}Fe. The sequence of single-particle levels obtained is close to that used in Ref. [4] for ^{82}Ge. For pairing gaps we obtain $\Delta_{p(n)} = 1.50(1.57)$ MeV for ^{76}Ge, $\Delta_{p(n)} = 1.59(1.42)$ MeV
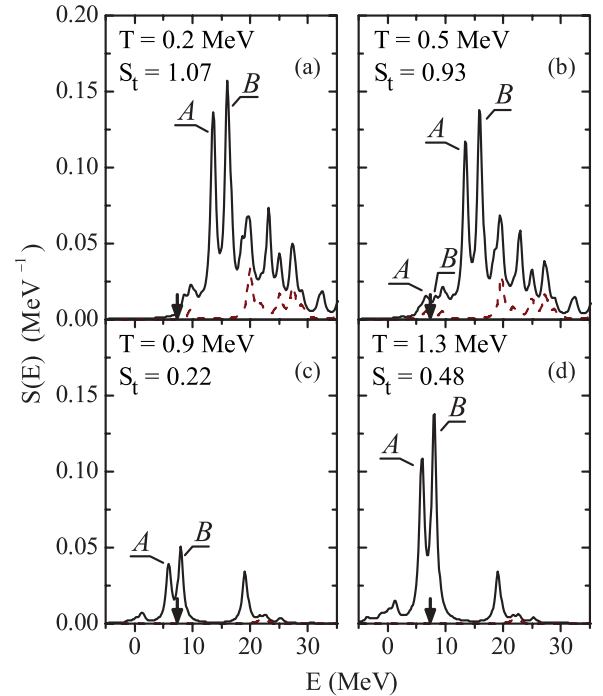
for ^{78}Ge, and $\Delta_{p(n)} = 1.39(1.35)$ MeV for ^{80}Ge. We take into account both the allowed (GT and Fermi) and the FF transitions with $J \leqslant 2$. To generate one-phonon states of natural and unnatural parity we use the isovector multipole and spin-multipole strength parameters $\kappa_1^{(\lambda)}$ and $\kappa_1^{(L\lambda)}$ ($\lambda = 0, 1, 2$) according to Refs. [42] and [43].

As a representative example, the strength distribution of allowed $p \rightarrow n$ transitions from ^{76}Ge for different values of temperature is displayed in Fig. 5. The distributions have been folded with a Breit-Wigner function of 1-MeV width. As follows from our study as well as from Refs. [4] and [20], two single-particle transitions mainly contribute to the total GT$_+$ strength in neutron-rich germanium isotopes. These are the $1g_{9/2}^p \rightarrow 1g_{7/2}^n$ particle-particle and $1f_{7/2}^p \rightarrow 1f_{5/2}^n$ hole-hole transitions. In an independent particle model both transitions are blocked at zero temperature. However, in the present model they become unblocked owing to pairing correlations and thermal excitations. Referring to Fig. 5 it is shown that, with increasing temperature, the peaks in the GT$_+$ distribution shift to lower excitation energies and the total strength decreases in the vicinity of the critical temperature ($T_{cr} \sim 0.8$ MeV).[3] The shift is about 8 MeV and, hence, cannot be explained solely by the removal of the extra energy needed to break a proton pair.

To explain both the effects we neglect the residual particle-hole interaction and consider the pairing interaction only.

_____

[3]The same effects were found in Ref. [28] for ^{80}Ge.

(As follows from our study, the position of the GT$_+$ peaks in ^{76,78,80}Ge is little affected by the inclusion of QRPA correlations and thermal one-phonon states can be considered as thermal two-quasiparticle states.) At finite temperature the GT$_+$ operator can excite configurations of four different types, namely, $[\beta_{j_p}^\dagger \beta_{j_n}^\dagger]_\mu^1$, $[\widetilde{\beta}_{\overline{j_p}}^\dagger \widetilde{\beta}_{\overline{j_n}}^\dagger]_\mu^1$, $[\widetilde{\beta}_{\overline{j_p}}^\dagger \beta_{j_n}^\dagger]_\mu^1$, and $[\widetilde{\beta}_{\overline{j_p}}^\dagger \beta_{j_n}^\dagger]_\mu^1$. The respective transition energies and transition strengths are

$$E_1(j_p \rightarrow j_n) = \varepsilon_{j_p} + \varepsilon_{j_n} + Q^*,$$
$$\Phi_1(j_p \rightarrow j_n) = \left(f_{j_p j_n}^1\right)^2 v_{j_p}^2 u_{j_n}^2 x_{j_p}^2 x_{j_n}^2;$$
$$E_2(j_p \rightarrow j_n) = -(\varepsilon_{j_p} + \varepsilon_{j_n}) + Q^*,$$
$$\Phi_2(j_p \rightarrow j_n) = \left(f_{j_p j_n}^1\right)^2 u_{j_p}^2 v_{j_n}^2 y_{j_p}^2 y_{j_n}^2; \qquad (23)$$
$$E_3(j_p \rightarrow j_n) = \varepsilon_{j_p} - \varepsilon_{j_n} + Q^*,$$
$$\Phi_3(j_p \rightarrow j_n) = \left(f_{j_p j_n}^1\right)^2 v_{j_p}^2 v_{j_n}^2 x_{j_p}^2 y_{j_n}^2;$$
$$E_4(j_p \rightarrow j_n) = -(\varepsilon_{j_p} - \varepsilon_{j_n}) + Q^*,$$
$$\Phi_4(j_p \rightarrow j_n) = \left(f_{j_p j_n}^1\right)^2 u_{j_p}^2 u_{j_n}^2 y_{j_p}^2 x_{j_n}^2.$$

Here $Q^* = \Delta\mu_{np} + \Delta m_{np}$ [see Eq. (20)]. In the following $j_p \rightarrow j_n$ refers to either the $1g_{9/2}^p \rightarrow 1g_{7/2}^n$ or the $1f_{7/2}^p \rightarrow 1f_{5/2}^n$ transition.

At $T < T_{cr}$ the excitation of the $[\beta_{j_p}^\dagger \beta_{j_n}^\dagger]_\mu^1$ configuration dominates the strength distribution because of the factor $x_{j_p}^2 x_{j_n}^2 \sim 1$ in $\Phi_1(j_p \rightarrow j_n)$. Therefore, at relatively low temperatures, when configuration mixing induced by pairing correlations in the ground state is the main unblocking mechanism, the position of the GT$_+$ peaks is given by $E_1(1g_{9/2}^p \rightarrow 1g_{7/2}^n)$ and $E_1(1f_{7/2}^p \rightarrow 1f_{5/2}^n)$ [Figs. 5(a) and 5(b)]. With increasing temperature states having internal configurations other than those of the nuclear ground state gain statistical weight, and in particular, the pairing correlations in these excited states decrease. When the pairing correlations disappear and the factors $v_{j_p}^2 u_{j_n}^2$ in $\Phi_1(j_p \rightarrow j_n)$ become zero, the peaks considered completely vanish [Fig. 5(c)]. The value of $\Phi_2(j_p \rightarrow j_n)$ becomes zero as well. At $T \geqslant T_{cr}$ the poles $\varepsilon_{1g_{9/2}^p} + \varepsilon_{1g_{7/2}^n}$ and $\varepsilon_{1f_{7/2}^p} + \varepsilon_{1f_{5/2}^n}$ no longer contribute to the secular equation (14).

At $T > T_{cr}$ GT$_+$ transitions from (to) thermally occupied (unblocked) orbitals dominate the strength distribution. These transitions correspond to excitation of the $[\widetilde{\beta}_{1g_{9/2}^p}^\dagger \beta_{1g_{7/2}^n}^\dagger]_\mu^1$ and $[\beta_{1f_{7/2}^p}^\dagger \widetilde{\beta}_{1f_{5/2}^n}^\dagger]_\mu^1$ configurations and their energies are $E_4(1g_{9/2}^p \rightarrow 1g_{7/2}^n)$ and $E_3(1f_{7/2}^p \rightarrow 1f_{5/2}^n)$, respectively. Neglecting Δm_{np}, these energies are the energy difference between the final and the initial single-particle states, that is, $E_4(1g_{9/2}^p \rightarrow 1g_{7/2}^n) \approx E_{1g_{7/2}^n} - E_{1g_{9/2}^p}$ and $E_3(1f_{7/2}^p \rightarrow 1f_{5/2}^n) \approx E_{1f_{5/2}^n} - E_{1f_{7/2}^p}$. Because of the thermally unblocked transitions the GT$_+$ peaks appear near the zero-temperature threshold [Fig. 5(d)].

Thus, in contrast to Ref. [20], we find that the unblocking effect for GT$_+$ transitions in neutron-rich nuclei is sensitive to increasing temperature. No shift to lower excitation energies for the GT$_+$ peaks or decrease in the total GT$_+$ strength in the vicinity of the critical temperature were observed in Ref. [20]. To understand these differences we compare

again the approximations underlying the present model and the hybrid approach used in Ref. [20]. The TQRPA has the virtue of consistency. It describes correlations by configuration mixing derived from a pairing interaction up to the 2p2h level. In the hybrid model, occupation numbers at finite temperature are calculated within the SMMC approach, accounting for all many-body npnh correlations induced by a pairing + quadrupole residual interaction. These occupation numbers have then been used to define a thermal ground state that is the basis of an RPA approach to calculate the capture cross sections, considering only 1p1h excitations on the top of this ground state. Therefore the hybrid model does not include explicitly 2p2h pairing correlations when calculating strength distributions.

Repeating our previous observation, the TQRPA has two distinct transitions to overcome Pauli blocking. Using, for the sake of simplicity, the language of the independent-particle model in the TQRPA, GT transitions can occur from configuration-mixed states with 0p0h and 2p2h components. These transitions lead to excited states in which centroids are shifted by the excitation energy of two particles raised across the pf-sdg shell gap, which corresponds to about 8 MeV for ^{76}Ge. The two peaks shown in the TQRPA GT strength distribution in Figs. 5(a) and 5(b) correspond to these two transitions. As the 2p2h component has two neutron holes, GT transitions into these holes are not Pauli blocked. Hence these transitions are relatively strong within the TQRPA model at low temperatures. On the other hand, GT transitions between pure 0p0h components are Pauli blocked. Transitions to final states corresponding to the lower centroid are only possible owing to the small mixing of 2p2h configurations into the final states. Hence the GT strength corresponding to the lower peak is rather weak at low temperatures [Fig. 5(b)]. The relative weight of the transition strength between these two peaks changes with increasing temperature owing to the increasing thermal excitations and the decreasing correlations induced by pairing. The latter effect dominates at modest temperatures. As a consequence, the strength in the upper peak decreases, whereas that of the lower peak increases and, at temperatures beyond the critical temperature T_{cr}, dominates the GT strength distribution in the TQRPA model [Fig. 5(d)].

It is found that in the SMMC approach many-body correlations lead to much stronger excitation of particles (mainly neutrons) across the pf-sdg shell gap than found in the TQRPA model. This is demonstrated in Figs. 6(a)–6(d), which compare the SMMC and thermal BCS occupation numbers for various orbitals as a function of temperature. Whereas the BCS predicts only 0.3 neutron to be excited out of the pf shell at $T = 0$ for ^{76}Ge, this number is about 1.2 for the SMMC, which is actually also smaller than the number of neutron excitations across the shell gap, recently derived experimentally (2.48 ± 0.30) [44]. Obviously, the differences in occupation numbers lead to the larger Pauli unblocking in the SMMC approach than found in the TQRPA model. Correspondingly, the RPA calculation on top of the SMMC occupation numbers predicts more GT strength in the energy range around 10 MeV (corresponding to the 0p0h centroid in the TQRPA calculation), which, as we show later, also results in higher capture cross sections at low temperatures.
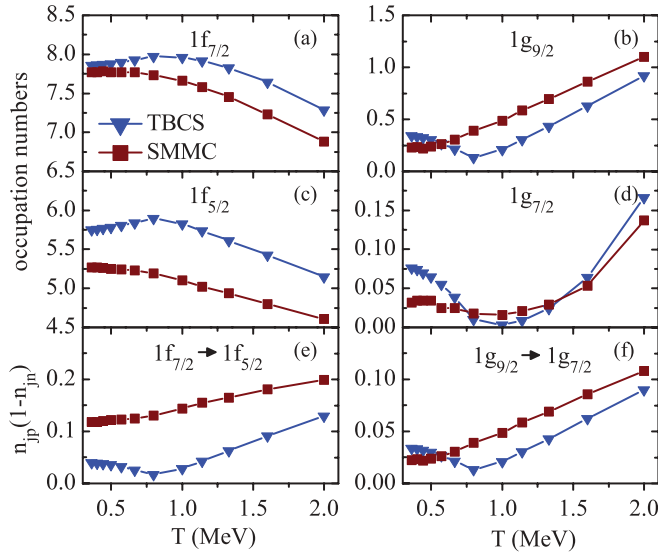
FIG. 6. (Color online) (a, b) Occupation numbers for the $1f_{7/2}$ and $1g_{9/2}$ proton orbitals in ^{76}Ge as a function of temperature. (c, d) Occupation numbers for the $1f_{5/2}$ and $1g_{7/2}$ neutron orbitals. (e, f) The unblocking probabilities for the $1f_{7/2}^{p} \rightarrow 1f_{5/2}^{n}$ and $1g_{9/2}^{p} \rightarrow 1g_{7/2}^{n}$ transitions.

In passing we note that, at low temperatures, the SMMC predicts a larger number of neutron excitations, but a smaller number of proton excitations, across the pf-sdg shell gap than the TQRPA model does. This highlights the importance of pn correlations, induced by isovector pairing and quadrupole interactions, in the SMMC approach. These types of pn correlations are not considered in the present TQRPA calculations.

In the SMMC, the many-body correlations induced by the "pairing+quadrupole" interaction also yield a significantly smaller temperature dependence in the occupation numbers than observed in the TQRPA approach. In this model, the energies of the unblocked GT_+ transitions essentially depend on temperature: at $T > T_{cr}$, when the unblocking is caused by thermal excitations (the thermal unblocking), they are smaller than the ones at $T < T_{cr}$, when the unblocking is caused by configuration mixing. Obviously, the significant shift of the GT_+ peaks to lower excitation energies favors EC. One can conclude that at $T > T_{cr}$ GT_+ transitions in neutron-rich nuclei are more unblocked than at $T < T_{cr}$.

To explain the second effect, we consider the total strength for the $j_p \rightarrow j_n$ transition,

$$S_t(j_p \rightarrow j_n) = \sum_i \Phi_i(j_p \rightarrow j_n) = \left(f_{j_p j_n}^1\right)^2 n_{j_p}(1 - n_{j_n}), \quad (24)$$

where n_{j_τ} is the proton ($\tau = p$) or neutron ($\tau = n$) occupation factor,

$$n_j = \langle 0(T); qp|a_{jm}^\dagger a_{jm}|0(T); qp\rangle = u_j^2 y_j^2 + v_j^2 x_j^2. \quad (25)$$

The value of $n_{j_p}(1 - n_{j_n})$ determines the unblocking probability for the $j_p \rightarrow j_n$ transition. As follows from Eq. (25) the unblocking probability depends on the temperature through the coefficients of both the Bogoliubov and the thermal transformation, that is, it is determined by both the configuration

mixing and the thermal excitations. We note again that at $0 < T < T_{cr}$ the total strength S_t of the unblocked particle-particle or hole-hole transition is not concentrated in only one peak but, as follows from Eq. (23), is fragmented into four parts. Figures 6(e) and 6(f) show the unblocking probabilities for the $1f_{7/2}^{p} \rightarrow 1f_{5/2}^{n}$ and $1g_{9/2}^{p} \rightarrow 1g_{7/2}^{n}$ transitions as a function of temperature.

As shown in Figs. 6(e) and 6(f) the unblocking probabilities for both transitions show a minimum at the critical temperature. It is apparent that this minimum occurs because at T_{cr}, pairing correlations vanish while thermal effects are not yet sufficiently strong to occupy the $1g_{9/2}$ proton orbit or unblock the $1f_{5/2}$ neutron orbit. As a result the total transition strength S_t decreases in the vicinity of the critical temperature. In contrast, this minimum is absent in the SMMC unblocking probabilities [see Figs. 6(e) and 6(f)]. Here the residual interaction introduces a slight, but gradual increase in the probability with temperature. At $T > 1.5$ MeV the SMMC and TQRPA results converge as is expected in the high-temperature limit.

The fact that crossing shell gaps by correlations is a rather slowly converging process that requires the consideration of multiparticle-multihole configurations has already been observed in large-scale diagonalization shell-model calculations, for example, studying calcium isotope shifts [45] or the M1 strength in argon isotopes [46].

For neutron-rich nuclei the contribution of the FF $p \rightarrow n$ transitions to EC is not negligible [4,20]. The strength distributions of FF 0^-, 1^-, and 2^- transitions in ^{76}Ge are shown in Fig. 7 for temperatures $T = 0.2$ and 1.3 MeV. The distributions have been folded by the same procedure used for the allowed transitions. As shown in the figure, a temperature increase weakly affects the peaks in the 0^- and 2^- strength distributions. The reason is that these are dominated by particle-hole transitions whose energy depends only weakly on temperature (in contrast to particle-particle and hole-hole transitions). With increasing temperature the peaks shift slightly to lower excitation energies owing to the vanishing of the pairing correlations, and some transition strength appears below the zero-temperature threshold owing to thermally unblocked transitions.

A finite temperature induces a significant spread in the 1^- transition strength distribution. The spread can be easily explained. At $T = 0.2$ MeV the main peak in the distribution is generated by three single-particle transitions: $1f_{7/2}^{p} \rightarrow 2d_{5/2}^{n}$, $1f_{5/2}^{p} \rightarrow 1g_{7/2}^{n}$, and $1f_{7/2}^{p} \rightarrow 1g_{9/2}^{n}$. The first is a particle-hole transition and its energy depends only slightly on temperature. The second and third are particle-particle and hole-hole transitions, respectively. As discussed above, the energies of particle-particle and hole-hole transitions are considerably lower at $T > T_{cr}$ than at $T < T_{cr}$. Therefore, at $T = 1.3$ MeV, the peak is fragmented into three parts, resulting in a broadening of the 1^- strength distribution. The 1^- peak at $E = 19$ MeV is generated by the particle-hole transition $1f_{7/2}^{p} \rightarrow 1g_{7/2}^{n}$, and hence, its position and strength almost do not depend on the temperature.

To reveal the importance of the thermal unblocking for GT_+ transitions in neutron-rich nuclei, we performed EC cross-section calculations. In the present approach, the total cross
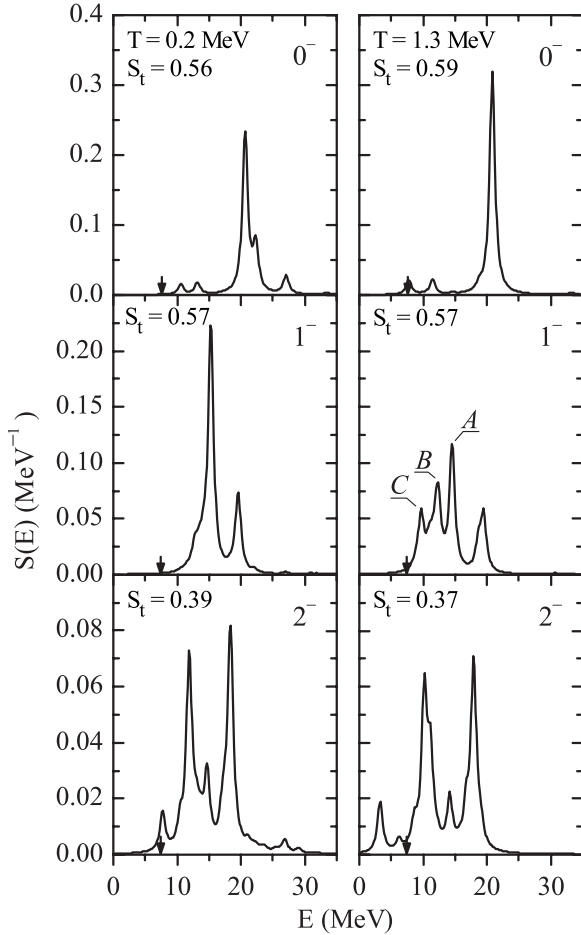
FIG. 7. Folded strength distributions of first-forbidden 0^-, 1^-, and 2^- $p \rightarrow n$ transitions in ^{76}Ge at $T = 0.2$ MeV (left panels) and $T = 1.3$ MeV (right panels); E is the transition energy. The strength distributions for the 2^- multipole correspond to 25-MeV electrons. S_t is the total strength. The arrows indicate the zero-temperature threshold. *A–C* label the 1^- transitions: $A \equiv 1f_{7/2}^p \rightarrow 2d_{5/2}^n$, $B \equiv 1f_{5/2}^p \rightarrow 1g_{7/2}^n$, $C \equiv 1f_{7/2}^p \rightarrow 1g_{9/2}^n$.

section for capture of an electron with energy E_e on a nucleus with charge Z is given by

$$\sigma(E_e, T) = \frac{G_w^2}{2\pi} F(Z, E_e) \sum_{Ji} (E_e - E_{Ji}^{(+)})^2 \Phi_{Ji}^{(+)}, \quad (26)$$

where G_w is the weak interaction coupling constant, and $F(Z, E_e)$ is the Fermi function that accounts for the Coulomb distortion of the electron wave function near the nucleus (see, e.g., Ref. [9]). Only allowed and FF transitions are involved in the sum over J in the present study.

In Fig. 8, the EC cross sections for ^{76,78,80}Ge are shown for three temperatures. The temperature dependence of the cross sections is most pronounced at moderate electron energies ($E_e \leqslant 15$ MeV): for $E_e = 15$ MeV a temperature increase from 0.5 to 1.3 MeV results in an enhancement of the cross sections by an order of magnitude. No such enhancement was found in Ref. [20] (see below). To make clear the reason for this enhancement, we calculate the relative contribution of allowed
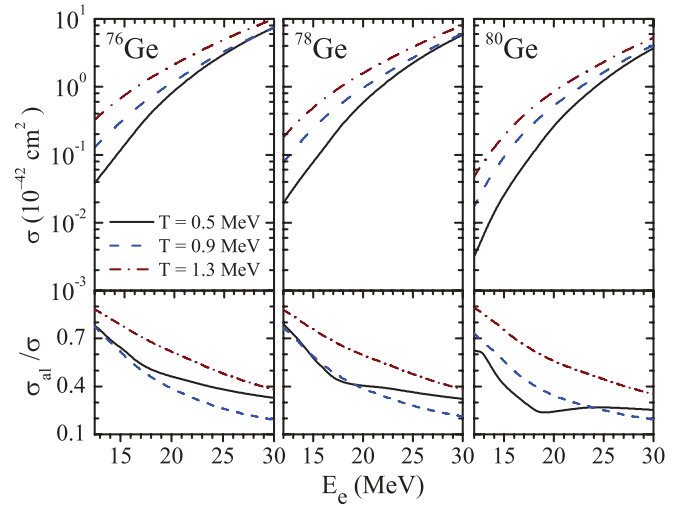

FIG. 8. (Color online) Electron capture cross sections (upper panels) for ^{76,80,80}Ge calculated within the TQRPA approach for various temperatures. Relative contributions of allowed transitions to the electron capture cross sections are shown in the lower panels.

transitions to the EC cross sections. The results are displayed in the lower panels in Fig. 8.

It is shown that at $E_e \leqslant 15$ MeV EC is mainly mediated by the allowed transitions. Consequently, the cross-section enhancement is caused by the thermal unblocking of GT$_+$ transitions (the Fermi contribution to the cross sections is negligible). Furthermore, because of the thermal unblocking, the electron energy below which EC is dominated by allowed transitions shifts to higher values: at $T = 0.5$ and 0.9 MeV this energy is 16–18 MeV, whereas at $T = 1.3$ MeV it is about 25 MeV. For higher electron energies, the FF transitions become increasingly important. As the strength of the FF transitions is less sensitive to temperature, the capture cross sections at $E_e \sim 30$ MeV depend only weakly on temperature.

The strong temperature sensitivity of the cross sections at low electron energies reflects the temperature dependence of the TQRPA GT strength distribution, as discussed previously. This has two main reasons. First, at low temperatures the dominant GT strength resides at higher excitation energies than in the hybrid model. Second, in the TQRPA the GT centroid shifts by several mega–electron volts, which is not observed in the hybrid model. Both facts, amplified by the strong phase-space energy dependence, lead to a much stronger dependence of the cross section in the TQRPA model than in the hybrid model. As the GT contribution to the cross sections is larger in the hybrid model than in the present TQRPA calculation, allowed transitions dominate to higher electron energies in the former.

Figure 9 compares the capture rates for ^{76,78,80}Ge as obtained in the hybrid and the TQRPA models. We note that the hybrid model rates are noticeably higher than the present rates at low temperatures. This is because of the increased unblocking probability in the hybrid model caused by many-body correlations, which lead to a greater GT strength at lower excitation energies than in the TQRPA approach. With increasing temperature and density the differences between the
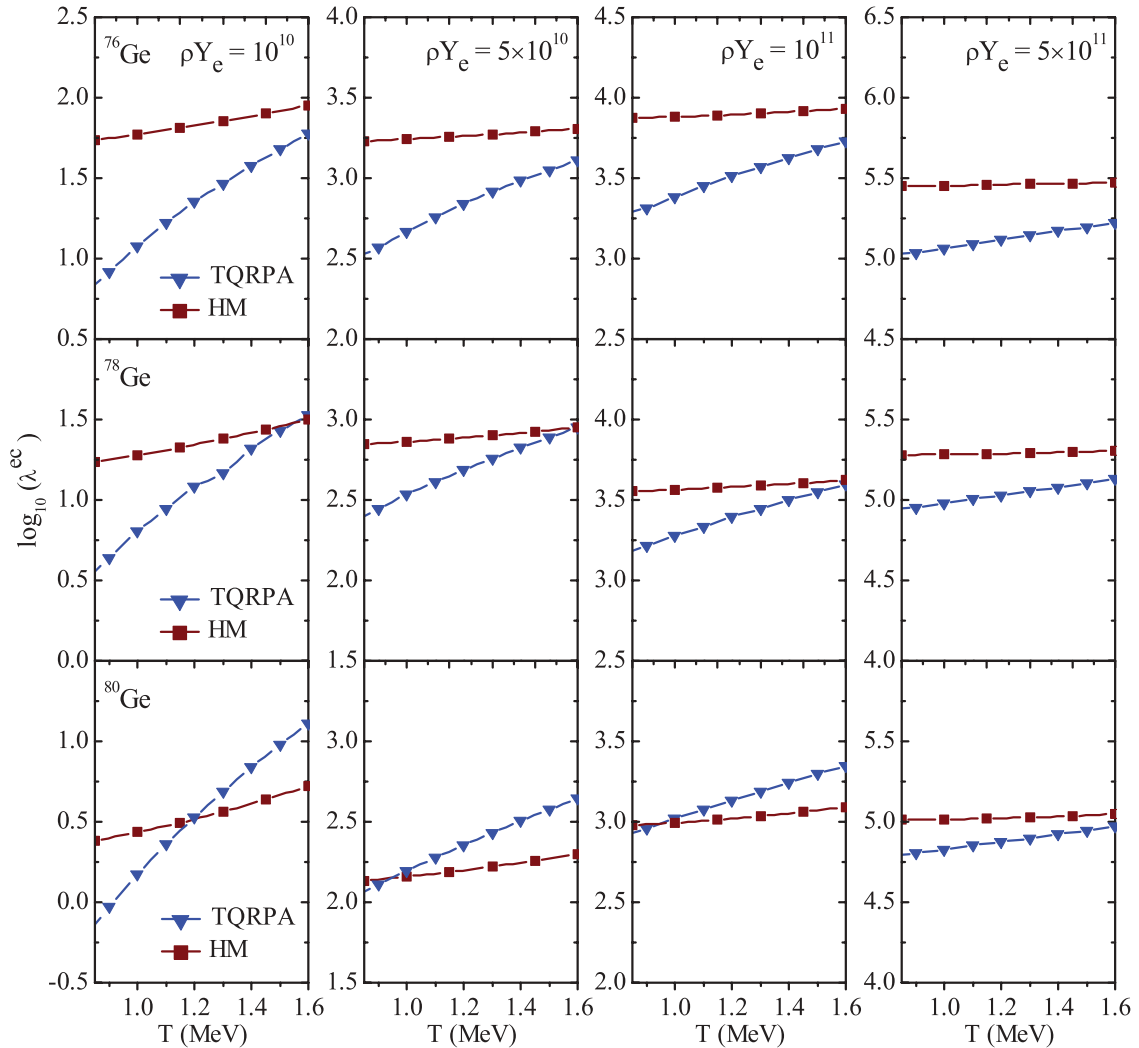
FIG. 9. (Color online) Electron capture rates for ^{76,78,80}Ge calculated using the TQRPA approach as a function of temperature and for selected values of density ρY_e (g cm^{-3}). For comparison, the rates obtained with the hybrid model (HM) are also shown.

rates in the two models become smaller. This has two causes. First, with increasing temperature and density the average electron energy increases and the rates become less sensitive to details of the GT strength distribution. Second, the GT strength distributions as calculated in the two models become more similar with increasing temperature as already discussed.

Note that the EC rates obtained in both models for the temperature and density regime when neutron-rich nuclei like those studied here dominate the composition during the supernova core collapse ($T > 1$ MeV, $\rho > 5 \times 10^{10}$ g/cm^3) are high enough that EC on nuclei dominates over capture on free protons as predicted in Ref. [20].

VI. CONCLUSION

In the present work, we have considered the GT$_+$ and FF transitions in hot nuclei. We have applied the proton-neutron QRPA extended to finite temperature by the TFD formalism. The approach allows treatment of charge-exchange transitions in nuclei at finite temperature, avoiding Brink's hypothesis. Moreover, the Ikeda sum rule was proven to be fulfilled at

finite temperature. As an example, the strength distributions of GT$_+$ transitions in ^{54,56}Fe have been calculated. A downward shift in the GT$_+$ strength was observed with increasing temperature. The shift is caused by the disappearance of pairing correlations and the appearance of negative- and low-energy transitions. The downward shift results in higher EC rates at high temperatures compared to those obtained in the shell-model calculations. We have found that the contribution of negative- and low-energy transitions, which are treated as transitions from thermally excited nuclear states, to EC is non-negligible even at low temperatures.

The GT$_+$ strength distribution in the neutron-rich ^{76,78,80}Ge nuclei have been calculated as well. It was found that the temperature increase leads to a considerable ($\sim$8-MeV) downward shift of the strength distribution peaks and reduces the total transition strength in the vicinity of the critical temperature. This makes the unblocking effect for neutron-rich nuclei in our model quite sensitive to increasing temperature, which is clearly observed in the EC cross sections and rates for ^{76,78,80}Ge.

Our results have been compared with those obtained within the shell-model diagonalization method for iron isotopes and within the hybrid SMMC + RPA model for the neutron-rich germanium isotopes. The importance of many-body correlations beyond those induced by pairing in our TQRPA model become apparent from the comparison. For the nuclides ^{54,56}Fe the Pauli unblocking is unimportant, as GT transitions are possible even in the independent-particle model without correlations. The TQRPA describes the centroid of the GT strength rather well. However, it misses the low-lying GT strength, which is induced by multinucleon correlations. The low-lying GT strength in ^{54,56}Fe that is observed experimentally and reproduced by the shell model is important for EC rates at low temperatures. Because of the lack of this part of the GT strength distribution, the EC rates are underestimated.

Pauli unblocking is crucial for calculation of the GT strength and the associated EC rates for the neutron-rich germanium isotopes. Previous calculations in the shell-model diagonalization method have shown that such cross-shell effects are rather slowly converging with increasing correlations across the shell gap and require the consideration of multinucleon correlations. This is in line with the observation that the SMMC approach, which accounts for complex configuration mixing, recovers significantly more excitations across the pf-sdg shell gap than found in the TQRPA approach, which, at low temperatures, derives the Pauli unblocking mainly from (2p2h) pairing correlations. As a result, the two approaches predict different GT distributions and capture rates at low temperatures and densities. On the contrary, both yield rather similar capture rates for collapse conditions where Pauli unblocking matters, confirming that capture on nuclei dominates over that on free protons.

In summary, we have presented an approach that allows calculation of stellar weak-interaction processes at finite temperature in a thermodynamically consistent way. This makes it conceptually superior to the hybrid approach of the SMMC + RPA, which has been used previously to estimate EC rates for neutron-rich nuclei. In the present application, correlations described by the TQRPA have been taken into account. Whereas much of the essential physics is already recovered, the detailed comparison to the shell-model results implies that the approach should be further improved. On the one hand, the predictive power is limited by the use of a phenomenological Hamiltonian consisting of a Woods-Saxon potential with locally readjusted depths as well as schematic residual interactions. Of particular importance is the inclusion of the attractive spin-isospin interaction in the particle-particle channel (see, e.g., Refs. [47] and [48]), which moves the GT strength to lower excitation energies. It would therefore be desirable to combine our TFD-based approach at finite temperature with self-consistent QRPA calculations based on more realistic effective interactions, including the particle-particle channel consistently (see, e.g., Ref. [49]). These improvements would also allow the effects of nuclear deformation to be properly taken into account [50]. Another direction is the inclusion of correlations beyond the RPA (or QRPA) by coupling the RPA phonons to more complex (e.g., two-phonon) configurations. For charge-exchange excitations in cold nuclei this problem has been considered within the QPM [30,31] and by approaches that solve the (second) RPA equations in the space of two-particle/two-hole excitations [51]. It was found that the coupling with complex configurations strongly fragments the RPA strength distribution.

We would like to reiterate that the present study can only be considered a first step toward reliable predictions of EC rates in nuclei not accessible to the shell model. Improvements along the lines discussed here will be made in future extensions of the model within the TFD framework.

[1] M. Di Toro, V. Baran, M. Cabibbo, M. Colonna, A. B. Larionov, and N. Tsoneva, Phys. Part. Nuclei **31**, 433 (2000).

[2] S. Shlomo and V. M. Kolomietz, Rep. Prog. Phys. **68**, 1 (2005).

[3] K. Langanke and G. Martínez-Pinedo, Rev. Mod. Phys. **75**, 819 (2003).

[4] J. Cooperstein and J. Wambach, Nucl. Phys. **A420**, 591 (1984).

[5] G. M. Fuller, W. A. Fowler, and M. J. Newman, Astrophys. J. Suppl. Ser. **42**, 447 (1980); **48**, 279 (1982); Astrophys. J. **252**, 715 (1982); **293**, 1 (1985).

[6] M. B. Aufderheide, I. Fushiki, S. E. Woosley, and D. H. Hartmann, Astrophys. J. Suppl. Ser. **91**, 389 (1994).

[7] K. Langanke and G. Martínez-Pinedo, Phys. Lett. **B436**, 19 (1998).

[8] K. Langanke and G. Martínez-Pinedo, Phys. Lett. **B453**, 187 (1999).

[9] E. Caurier, K. Langanke, G. Martínez-Pinedo, and E. Nowacki, Nucl. Phys. **A653**, 439 (1999); K. Langanke and G. Martínez-Pinedo, *ibid.* **A673**, 481 (2000).

[10] K. Langanke and G. Martínez-Pinedo, At. Data Nucl. Data Tables **79**, 1 (2001).

[11] K. Kar, A. Ray, and S. Sarkar, Astrophys. J. **434**, 662 (1994).

[12] J.-U. Nabi and H. V. Klapdor-Kleingrothaus, At. Data Nucl. Data Tables **88**, 237 (2004).

[13] N. Paar, G. Coló, E. Khan, and D. Vretenar, Phys. Rev. C **80**, 055801 (2009).

[14] S. E. Koonin, D. J. Dean, and K. Langanke, Phys. Rep. **278**, 1 (1997).

[15] P. B. Radha, D. J. Dean, S. E. Koonin, K. Langanke, and P. Vogel, Phys. Rev. C **56**, 3079 (1997).

[16] A. Juodagalvis, K. Langanke, W. R. Hix, G. Martinez-Pinedo, and J. M. Sampaio, arXiv:0909.0179v1 [nucl-th].

[17] J. A. Halbleib and R. A. Sorensen, Nucl. Phys. **A98**, 542 (1967).

[18] Y. Takahashi and H. Umezawa, Collect. Phenom. **2**, 55 (1975).

[19] H. Umezawa, H. Matsumoto, and M. Tachiki, *Thermo Field Dynamics and Condensed States* (North-Holland, Amsterdam, 1982).

[20] K. Langanke, E. Kolbe, and D. J. Dean, Phys. Rev. C **63**, 032801(R) (2001).

[21] K. Tanabe, Phys. Rev. C **37**, 2802 (1988).

[22] T. Hatsuda, Nucl. Phys. **A492**, 187 (1989).

[23] O. Civitarese and A. L. DePaoli, Z. Phys. A **344**, 243 (1993).

[24] D. S. Kosov and A. I. Vdovin, Mod. Phys. Lett. A **9**, 1735 (1994).

[25] D. S. Kosov, A. I. Vdovin, and J. Wambach, in *Proceedings of the International Conference on Nuclear Structure and Related Topics, Dubna, 1997*, edited by S. N. Ershov, R. V. Jolos, and V. V. Voronov (Joint Institute for Nuclear Research, Dubna, 1997), E4-97-327, p. 254.

[26] I. Ojima, Ann. Phys. **137**, 1 (1981).

[27] A. A. Dzhioev and A. I. Vdovin, Int. J. Mod. Phys. E **18**, 1535 (2009).

[28] A. A. Dzhioev, A. I. Vdovin, V. Yu. Ponomarev, and J. Wambach, Yad. Fiz. **72**, 1373 (2009) [Phys. At. Nucl. **72**, 1320 (2009)].

[29] V. G. Soloviev, *Theory of Atomic Nuclei: Quasiparticles and Phonons* (Institute of Physics, Bristol, UK, 1992).

[30] V. A. Kuzmin and V. G. Soloviev, J. Phys. G **10**, 1507 (1984).

[31] V. A. Kuzmin and V. G. Soloviev, J. Phys. G **11**, 603 (1985).

[32] A. L. Goodman, Nucl. Phys. **A352**, 30 (1981).

[33] O. Civitarese, G. G. Dussel, and R. P. J. Perazzo, Nucl. Phys. **A404**, 15 (1983).

[34] O. Civitarese and M. Reboiro, Phys. Rev. C **63**, 034323 (2001).

[35] A. Heger, S. E. Woosley, G. Martínez-Pinedo, and K. Langanke, Astrophys. J. **560**, 307 (2001).

[36] V. A. Chepurnov, Yad. Fiz. **6**, 955 (1967) [Sov. J. Nucl. Phys. **6**, 696 (1968)].

[37] K. Pomosrki, P. Ring, G. A. Lalazissis, A. Baran, Z. Lojewski, B. Nerlo-Pomorska, and M. Warda, Nucl. Phys. **A624**, 349 (1997).

[38] G. Audi and A. H. Wapstra, Nucl. Phys. **A565**, 1 (1993).

[39] J. Rapaport, T. Taddeucci, T. P. Welch, C. Gaarde, J. Larsen, D. J. Horen, E. Sugarbaker, P. Koncz, C. C. Foster, C. D. Goodman, C. A. Goulding, and T. Masterson, Nucl. Phys. **A410**, 371 (1983).

[40] T. T. Rönnqvist, H. Condé, N. Olsson, E. Ramström, R. Zorro, J. Blomgren, A. Håkansson, A. Ringbom, G. Tibell, O. Jonsson, L. Nilsson, P.-U. Renberg, S. Y. van der Werf, W. Unkelbach, and F. P. Brady, Nucl. Phys. **A563**, 225 (1993).

[41] S. El-Kateb, K. P. Jackson, W. P. Alford, R. Abegg, R. E. Azuma, B. A. Brown, A. Celler, D. Frekers, O. Häusser, R. Helmer, R. S. Henderson, K. H. Hicks, R. Jeppesen, J. D. King, K. Raywood, G. G. Shute, B. M. Spicer, A. Trudel, M. Vetterli, and S. Yen, Phys. Rev. C **49**, 3128 (1994).

[42] B. Castel and I. Hamamoto, Phys. Lett. **B65**, 27 (1976).

[43] D. R. Bes, R. A. Broglia, and B. S. Nilsson, Phys. Rep. **16**, 1 (1975).

[44] J. P. Schiffer, S. J. Freeman, J. A. Clark, C. Deibel, C. R. Fitzpatrick, S. Gros, A. Heinz, D. Hirata, C. L. Jiang, B. P. Kay, A. Parikh, P. D. Parker, K. E. Rehm, A. C. C. Villari, V. Werner, and C. Wrede, Phys. Rev. Lett. **100**, 112501 (2008).

[45] E. Caurier, K. Langanke, G. Martínez-Pinedo, F. Nowacki, and P. Vogel, Phys. Lett. **B522**, 240 (2001).

[46] A. F. Lisetskiy, E. Caurier, K. Langanke, G. Martínez-Pinedo, P. von Neumann-Cosel, F. Nowacki, and A. Richter, Nucl. Phys. **A789**, 114 (2007).

[47] V. A. Kuzmin and V. G. Soloviev, Nucl. Phys. **A486**, 118 (1988).

[48] P. Sarriguren, R. Álvarez-Rodríguez, and E. Moya de Guerra, Eur. Phys. J. A **24**, 193 (2005).

[49] J. Engel, M. Bender, J. Dobaczewski, W. Nazarewicz, and R. Surman, Phys. Rev. C **60**, 014302 (1999).

[50] P. Sarriguren, E. Moya de Guerra, and A. Escuderos, Nucl. Phys. **A691**, 631 (2001).

[51] S. Drożdż, V. Klemt, J. Speth, and J. Wambach, Phys. Lett. **B166**, 18 (1986); S. Drożdż, F. Osterfeld, J. Speth, and J. Wambach, *ibid.* **B189**, 271 (1987).